energies

MDPI

Article

Determination of the Soiling Impact on Photovoltaic Modules at the Coastal Area of the Atacama Desert

Douglas Olivares [1], Pablo Ferrada [1,*], Jonathan Bijman [1], Sebastián Rodríguez [1], Mauricio Trigo-González [1], Aitor Marzo [1], Jorge Rabanal-Arabach [2], Joaquín Alonso-Montesinos [3,4], Francisco Javier Batlles [3,4] and Edward Fuentealba [1]

1 Centro de Desarrollo en Energías Antofagasta, Universidad de Antofagasta, Av. Universidad de Antofagasta #02800, Antofagasta 1271155, Chile; douglas.olivares@uantof.cl (D.O.); jonathanbijman@gmail.com (J.B.); sebastian.rodriguez@uantof.cl (S.R.); mauricio.trigo@uantof.cl (M.T.-G.); aitor.marzo@uantof.cl (A.M.); edward.fuentealba@uantof.cl (E.F.)

2 Departamento de Ingeniería Eléctrica, Universidad de Antofagasta, Avenida Angamos 601, Antofagasta 1270300, Chile; jorge.rabanal@uantof.cl

3 Departamento de Química y Física, Universidad de Almería, 04120 Almería, Spain; joaquin.alonso@ual.es (J.A.-M.); fbatlles@ual.es (F.J.B.)

4 CIESOL, Joint Centre of the University of Almeria CIEMAT, 04120 Almería, Spain

* Correspondence: pablo.ferrada@uantof.cl; Tel.: +56-55-2-513530

Received: 1 June 2020; Accepted: 22 July 2020; Published: 24 July 2020

Abstract: With an elevation of 1000 m above sea level, once the coastal mountain range is crossed, the Atacama Desert receives the highest levels of solar radiation in the world. Global horizontal irradiations over 2500 kWh/(m^2 year) and a cloudiness index below 3% were determined. However, this index rises to 45% in the coastal area, where the influence of the Pacific Ocean exists with a large presence of marine aerosols. It is on the coastal area that residential photovoltaic (PV) applications are concentrated. This work presents a study of the soiling impact on PV modules at the coastline of Atacama Desert. The current–voltage characteristics of two multicrystalline PV modules exposed to outdoor conditions were compared, while one of them was cleaned daily. Asymptotic behavior was observed in the accumulated surface dust density, over 6 months. This behavior was explained by the fact that as the glass became soiled, the probability of glass-to-particle interaction decreased in favor of a more likely particle-to-particle interaction. The surface dust density was at most 0.17 mg·cm^{-2} per month. Dust on the module led to current losses in the range of 19% after four months, which in turn produced a reduction of 13.5%$_{rel}$ in efficiency.

Keywords: soiling; glass; PV modules; module temperature; current–voltage characteristics

1. Introduction

The Atacama Desert is one of the places with the world's highest solar radiation indices. In addition, it is characterized by a great number of sunny days, with a cloud index lower than 3% in non-coastal areas and a low content of aerosols, water vapor, and ozone in the atmosphere [1]. These conditions make it an ideal place for developing solar projects. However, most urban areas are located on the coastline, between the ocean and the coastal mountains. The climatic conditions of the desert, the industry, and the strong influence of the Pacific Ocean on this area, pose important challenges for the optimal operation of energy generated through photovoltaic (PV) systems. One of these problems is the soiling effect on the PV module surface [2].

Dust deposited on the PV modules reduces the number of photons reaching the solar cells. In other words, soiling reduces the glass capacity to transmit photons, i.e., its transmittance [3–5]. Thus, transmittance loss results from the absorption and reflection of the incident light by the deposited

material and the glass. These phenomena result in power loss and, therefore, economic loss. PV module soiling is a world problem and an area of increasing concern in performance and financial return [6]. For all these reasons, the topic was, and is, widely discussed in the literature over the last decade. According to SCOPUS [https://www.scopus.com], the number of papers published in "soiling" and "photovoltaics" in the years 2018 and 2019, represents about 40% of the total number of papers published (see Figure 1).

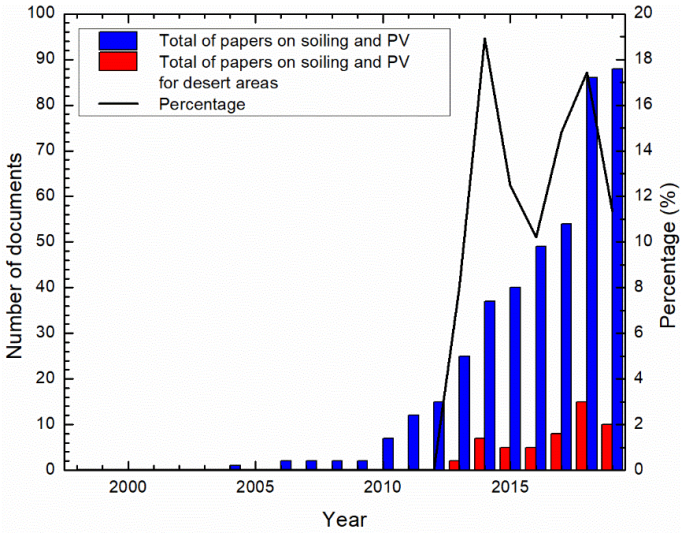

Figure 1. Number of papers published in the last 20 years according to the Scopus source under the search terms "soiling" and "photovoltaics", and "soiling" and "photovoltaics" and "desert". The full line represents the percentage of papers published on the subject of deserts, compared to the total.

Accumulation of soiling and the losses caused are phenomena greatly depending on the local environment and the type of PV technology. The daily amount of deposited soiling, soiling rate, or daily dust accumulation, depends on environmental conditions, kind of surface, atmospheric dust concentration, dust chemical composition, distance to dirt sources, and rainfall, among others [7]. Therefore, the processes of dust accumulation depend particularly on three factors—the weather conditions, the type of dust, and the characteristics of the photovoltaic installation.

The problem of soiling is especially important in arid areas. As the places where there are more solar resources generally coincide with arid and desert areas, where there is an abundant amount of dust, the interest of studies centered on these zones has increased in the past years (see Figure 1). Water, which is scarce in desert areas, plays an important role in the process of soiling and cleaning of the PV panels. On the one hand, water is used for the cleaning tasks of PV modules. In areas with abundant rainfall, this rain helps to naturally clean the PV modules of the dust and dirt accumulated on their surfaces. On the other hand, moisture is known to play an important role in the cementing process, especially if the deposited material is soluble and hygroscopic, which increases the adhesion of the particles to the glass surface, thus, contributing to the cementing process [3,8]. Thus, in coastal areas of deserts, the problem of soiling can be exacerbated by low rainfall, abundance of salts, and high levels of atmospheric humidity, due to proximity to the ocean.

A recent study of soiling in desert areas carried out by Said et al. [9] concluded that the amount of dust accumulated after 45 days of exposure in Dhahran was 0.5 mg·cm^{-2}, which reduced the transmittance of its photovoltaic glass by 20%. With regards to the photogenerated current, Qasem et al. [10] found that amorphous silicon (a-Si) technologies showed a 33% decrease for a dust density of 4.25 mg·cm $^{-2}$, while for crystalline silicon (c-Si) modules, it decreased by 28.6%. In both cases, the voltage was not substantially affected. These studies are some of the examples that show a direct correlation between energy loss and the surface dust density of the photovoltaic modules.

Other studies throughout the world reveal that dust accumulation is responsible for a significant loss of energy conversion [11,12]. A 0.3% energy loss caused by dust was reported in Libya and Mountain View; 0.6% in Abu Dhabi; 0.8% in Ogbomosho, and 1.2% in Dhaka, Kuwait, and Riyadh. In the case of the Atacama Desert, Araya et al. [13] studied the performance ratio (PR) for different places, such as coastal locations, an industrial site, and the highlands. For a period of 12 months, PR decrease was found to be greater for multi crystalline silicon technology (mc-Si, 47%), as compared to cadmium telluride (CdTe, 46%) on the coastal zone. Araya et al. indicated that amorphous/microcrystalline silicon (a-Si/µc-Si) thin-films resulted in a greater PR decrease, followed by mc-Si (39%), where the smallest decrease occurred with mono crystalline Si modules (36%), which were also located on the coastal desert zone. The same calculation for modules installed in the industrial zone at the inner region of the desert resulted in a PR of 35% for CdTe, 49% for mc-Si, and 47% for mc-Si with single-axis tracking. The rate at which PR decreased with time, depended on technology, installation, temperature, and location. Other studies showed similar results for c-Si, mc-Si, and a-Si/µc-Si thin-film technologies installed in the coastal areas of the Atacama Desert [13,14].

It is well-known that silicon solar cells are sensitive to temperature variations. Therefore, the PV module voltage, current, and, therefore, its PR, are affected by the temperature of the cell matrix. Variation due to temperature is significant in the open circuit voltage (V_{oc}) [15]. Hence, the fill factor (FF) and PR are strongly influenced by the temperature of the device, owing to its dependence on V_{oc}. In this way, the relationship between the short-circuit current (corrected temperature) and the irradiance at the plane of array (I_{sc}/G_{poa}) is recommended as a metric for determining the influence of soiling [16].

The main objective of this study was to determine the soiling effects on the PV modules installed at the coastal zone of the Atacama Desert. To do this end, the characteristic current–voltage (IV) curve was measured in two conditions—(1) a module that was cleaned daily (clean module); and (2) a module that allowed getting natural soiling (dirty module). Additionally, the surface dust density on the PV glass was measured as function of time. Since the ambient and module temperature play a fundamental role during the IV curve measurement process, the temperature was estimated and compared with the module temperature measure to validate the correction made by the IV curve tracer.

This study contributed to the field with the proposal of a methodology to conduct technical studies on PV module soiling and electrical performance, by measuring the IV curve. It also helped the user utilize the PV system maintenance program through predictive planning, based on the climatic conditions of the environment and the sky. The soiling losses of the coastal area of the Atacama Desert were quantified and their behavior was analyzed, according to the climate of the zone. In addition, a methodology was presented to support temperature measurements based on an NREL (National Renewable Energy Laboratory of the United States) estimated model, with a linear adjustment quite close to 1.

2. Materials and Methods

2.1. Location

The PV modules tested were mounted at the facilities of University of Antofagasta (UA), located at −23.70° S, −70.42° W, on the coast of the Chilean portion of the Atacama Desert. This region had a BWn-type climate, according to Köppen's classification [17]. It corresponded to a coastal zone characterized by scarce rainfall and an extremely dry environment, making it an extremely arid area (Figure 2).

In this part of the Atacama Desert, two peculiar phenomena occur. One of them was the Humboldt current and its morphological geography [18]. This current was characterized by a considerable cooling influence on the Atacama Desert climate. The cool sea current in deep water, running along almost the whole Pacific Ocean coast in South America, prevents a high rate of water from evaporating, minimizing cloud formation over the ocean. The morphology of this region of the Atacama Desert

showed a slope from 0 to 5900 m.a.s.l. in just 250 km breadthways. Along this region, there are two mountain chains called Cordillera de la Costa (3100 m.a.s.l.) and Cordillera de Los Andes (5900 m.a.s.l.), which block the transit of clouds into the region. The Cordillera de la Costa also contributes to trap the coastal low-pressure systems between the marine boundary layer and the coastal mountains [19]. As a result, this zone is known as the driest non-polar temperate desert on Earth [20,21]. In the city of Antofagasta, maximum average temperatures of 24 °C and 16.9 °C are registered in summer and winter, respectively [18]. Throughout the year, accumulated rainfall is approximately 1.7 mm.

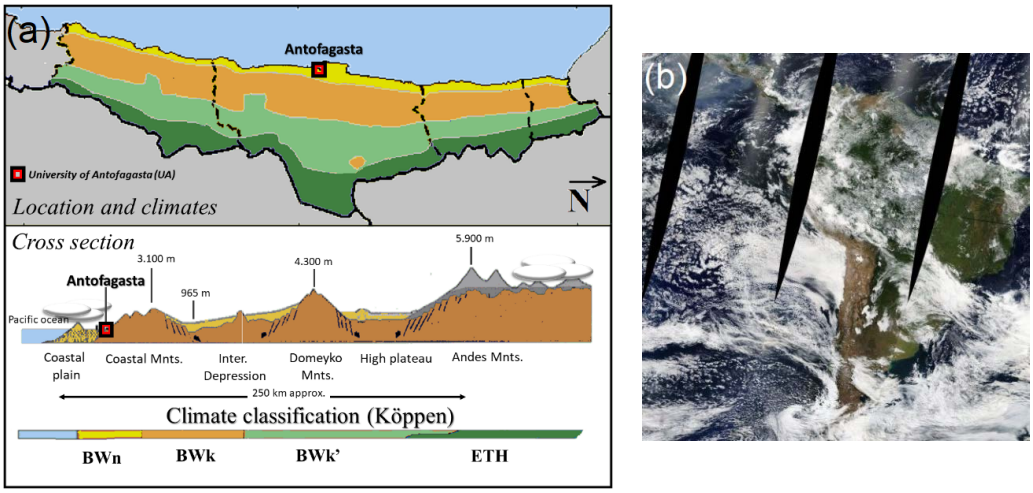

Figure 2. (**a**) University of Antofagasta (UA) campus, cross-section of the Antofagasta Region and climate classification, according to Köppen. Image based on [22]. (**b**) Picture taken by Terra satellite on 28 April 2019 [23], showing a portion of Atacama Desert.

2.2. Materials

Commercial mc-Si modules with 15.4% efficiency were used (BYD P6C-30 Series). These modules have a nominal power of 250 W, a short circuit current (I_{sc}) of 8.8 A, and an open circuit voltage (V_{oc}) of 37.9 V, occupying a 1.63 m^2 area. In this experiment, two modules of same characteristics were mounted on a north-facing aluminum structure with a 20° inclination. To measure the surface dust density, several glass samples of 6.5 cm × 4.5 cm were used. These samples were placed in a north-facing metal plate, with the same inclination as the PV modules.

2.3. Instrumentation

The PV modules were selected from a bunch by using thermography and electroluminescence (EL) techniques. The thermography was performed with a Fluke Ti32 camera to identify the presence of hotspots on the PV modules. The EL was conducted using a DC power supply Keysight N8941A, which can reach the required I_{sc} and V_{oc} values (~9 A and ~40 V). A modified commercial CCD camera, to which a long-pass filter (cut-on at 830 nm) was incorporated, enabled detection of the emitted radiation.

To obtain the characteristic electrical parameters, a commercial IV tracer (h.a.l.m. cetis PV-CT-F1) was used. This device swept the voltage over the PV module, which recorded the different current values over its IV curve. Sweeping can be made from V_{oc} to I_{sc} or vice versa. In this case, the sweep starts at $U = 0$ V ($I = I_{sc}$) and finishes at $U = V_{oc}$ ($I = 0$ A). To obtain more information from the IV curve, it is also necessary to know the solar irradiance and the module temperature at the moment of the voltage sweep. The irradiance was obtained with a reference cell (Si-02-PT1000-4L-X) placed at the module structure; whereas the ambient temperature was measured with a PT1000 sensor. When IV curves were measured, irradiance and module temperatures were as well measured, synchronically. It is important to emphasize that the reference cell incorporates a temperature sensor to perform

corrections of the measurements, due to its operating temperature. Such a correction is performed internally by the device, according to the IEC 60904-4. A weather station performing continuous records was used to validate the ambient temperature measurements. The equipment corresponded to a cup anemometer and a solar tracker, Solys2. The latter incorporated an ambient temperature sensor and a pyranometer type ISO 9060 spectrally flat Class A. The dust density was measured by gravimetric gain on a precision balance of the Vibra brand LF224R series, with an automatic range adjustment function to maintain high accuracy.

This work used images from a hemispheric low-cost sky camera, model Mobotix Q24. The images had a high resolution from a fully digital color CMOS (2048 × 1536 pixels). One image was recorded every minute in JPEG format, i.e., the optimal time to identify clouds in the sky. The three distinct channels represent red, green, and blue levels. Each image pixel is made up of 8 bits, obtaining values between 0 and 255.

2.4. Methodology

The procedure began by selecting two PV modules homogeneous among themselves, as shown in Figure 3, where *i* stands for days, *j* is for weeks, and *k* means months. The selected modules were later mounted on a 20° inclined rack, with respect to the horizontal plane. In addition, a metal plate with the same elevation and orientation was installed and several glasses were placed on it. The IV curves were subsequently measured over a period of six months, in addition to other parameters of interest (e.g., solar irradiance and module temperature). To validate temperature values measured at the back side of each PV module, recorded data were compared with the calculated module temperature, according to NREL [24] (see Equation (1)).

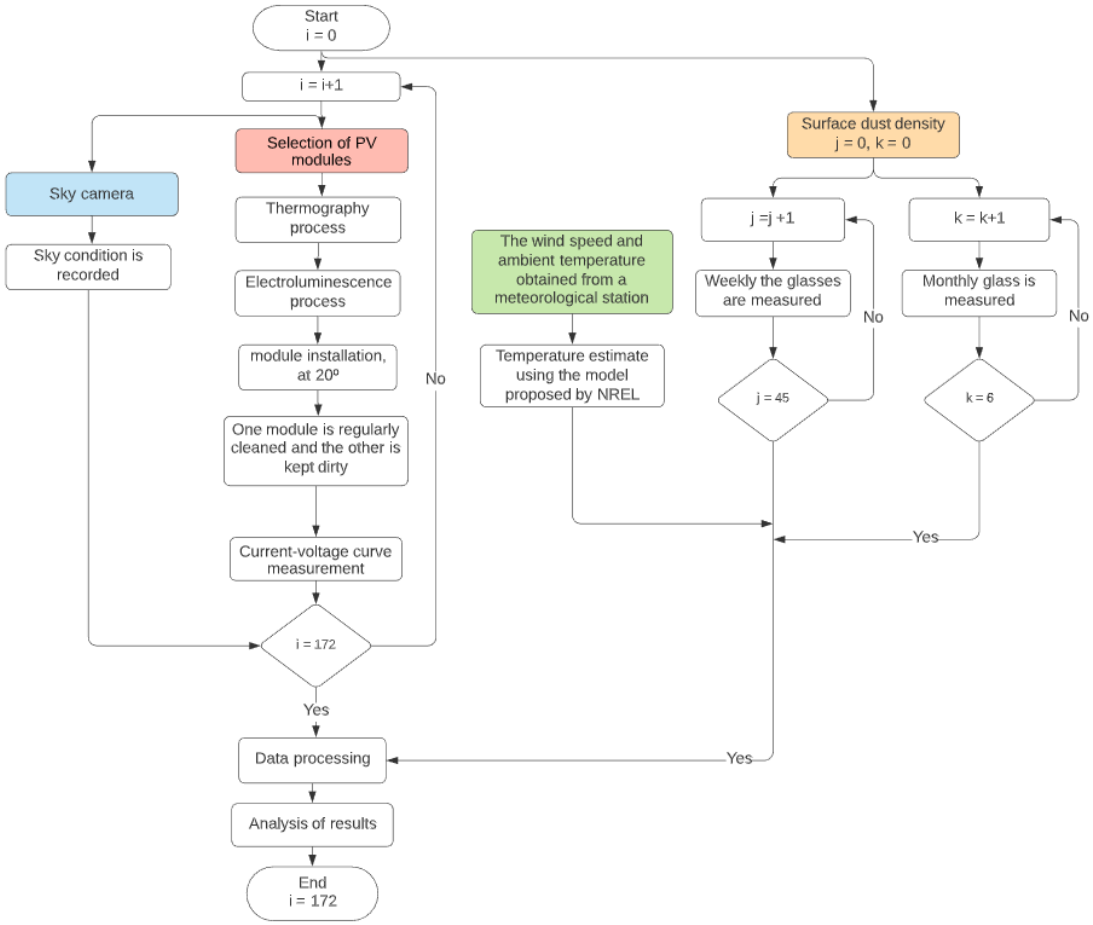

Figure 3. Flowchart illustrating the general procedure. An explanation for each box is given below.

2.4.1. PV Module Selection

To detect and reject faulty modules, an in-field thermographic-based study was conducted. In this case, 26 samples were analyzed. The modules were exposed to natural illumination in short-circuit mode, for 10 min. After the photovoltaic effect occurred in solar cells, there was an amount of energy that dissipated in the form of heat—the Joule effect. In addition, the glass and the encapsulant could also absorb a part of the incoming radiation, according to their respective absorption coefficients, and could produce heat. Such heat was transferred by conduction to the neighboring material, according to the thermal conductivity of the material and following the laws of thermodynamics.

Moreover, Stefan-Boltzmann's law states that every surface with a temperature greater than absolute zero emits radiation. This radiation, denoted as thermal irradiance (E), is a function of Stefan-Boltzmann (σ), the surface temperature (T), and its emissivity (ε), according to equation $E = \varepsilon\sigma T^4$. The thermographic cameras are sensitive to infrared irradiance. These can measure incident radiation over their sensors, E, and interpret it as temperature, by applying an adjustment function obtained from Stefan-Boltzmann's law and the surface body emissivity. Under the normal operational conditions of an undamaged module, all its solar cells respond in a similar manner to incident solar radiation, generating a certain equivalent voltage, current, and temperature. Consequently, the outer glass does not show temperature gradients and, hence, the thermographic image is homogeneous, as the one shown in Figure 4a. Nevertheless, if there is a failure on any of the cells (e.g., a broken cell), the defective cell gets hotter than the adjacent ones and transfers more heat to the outer glass, causing the thermography of the panel to not be completely homogeneous (Figure 4b). Therefore, the thermographic camera was used to detect thermal gradients on the glass, accounting for temperature variations among the solar cells.

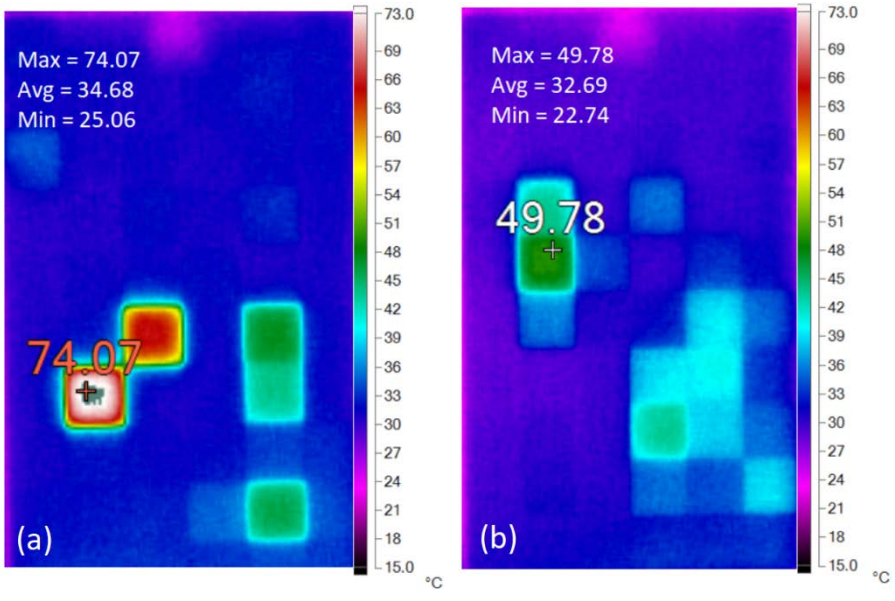

Figure 4. Images obtained with an infrared thermal camera. (**a**) Discarded module with hot areas; and (**b**) selected module without hotspots.

In this case, the spectral band measured by the camera was from 7.5 µm to 14 µm. The thermographic pictures of each module were taken independently, at an angle of 10° regarding the normal to the PV module. The process was conducted under natural light at noon, to maintain similar levels of irradiance and inclination. Fluke SmartView 4.3 software was used for image processing.

A second selection criterion consisted of EL pictures to discard modules whose solar cells showed fractures. The procedure was based on polarizing the modules with a DC power supply in a dark environment with controlled conditions (T ~ 25 °C and no light sources). The modules were

energized one by one with a 48 V voltage and an 8.8 A current for a short time. Once a module was powered, the semiconductor started emitting photons through a direct recombination of wavelengths corresponding to the material bandgap (~1150 nm for the devices based on c-Si). These photons were captured by a detector (CCD camera, in this case). The pictures were taken with 30 s of exposition and at 10°, with respect to the module normal.

2.4.2. Current-Voltage Curve Measurement

The IV curves were always obtained by considering one clean and one dirty PV module. The IV curves were measured for six months, obtaining the short-circuit current (I_{sc}), open-circuit voltage (V_{oc}), maximum power (P_{MPP}), efficiency (η), and module temperature (T_{mod}). The measurements were performed at solar noon and cloud intermittency; in data post-processing between measurements from one module to another was considered. To compare the current and power for different ambient conditions, the measurements were STC-adjusted by irradiance and temperature, using the correction procedure as per IEC 60891. For this, temperature coefficients of 0.07%/K and −0.33%/K were used for the current and voltage, respectively.

2.4.3. Temperature Measurement and Validation

To confirm the proper operation of the temperature sensor used by the IV tracer, a mathematical model was used. This model determined the temperature at the back of the PV module (Equation (1)), which considered the wind speed (W_S), ambient temperature (T_a), the broadband irradiance measured at the plane of the array (G_{POA}), the empirical constant that reflected the increase in module temperature with solar radiation (a), and the empirical constant reflecting the wind effect on the module temperature (b), as input data [24].

$$T_{mod} = G_{POA} e^{(a+bW_s)} + T_a \quad (1)$$

To obtain the wind speed, a cup anemometer model Young WIND Monitor 05,103 was used, along with a Vaisala HMP60 sensor, to obtain the ambient temperature data. Temperature was calculated for each position in the module.

2.4.4. Surface Dust Density

Two types of measurements on a weekly and monthly basis were made to have a higher resolution. The glass samples were weighed and returned to their original position, according to the weekly samples that were removed, once the dust was measured. For greater representativeness of the measurement, four samples were placed per measurement.

2.4.5. Sky Camera

To get more insight into the result, the sky was classified into three categories—(1) cloudy, (2) partially cloudy, and (3) overcast. Cloudy days did not appear in the period of the IV curve measurements. Partially cloudy days were defined as days with irradiance variations caused by clouds that appeared and disappeared quickly. Overcast days were classified according to cloud appearance during the period of IV curve measurement.

3. Results

3.1. Module Selection and Temperature Analysis

Six modules were chosen from the 26 original ones. They showed a more homogeneous distribution of cell temperature, as compared to the whole group (some modules showed cells with temperatures higher than the average measured, 74.1 °C, with a maximum difference of 24.3 °C, as shown in Figure 4, for example).

The results of EL imaging showed that at least 3 out of the 6 pre-selected thermography modules showed rows with lower emissivity and, hence, probably had a lower efficiency. The selection criterion established that, each photographed module should not have presented any case of lower emission that could result in a possible cell failure. Figure 5 shows how the module selection criteria were applied.

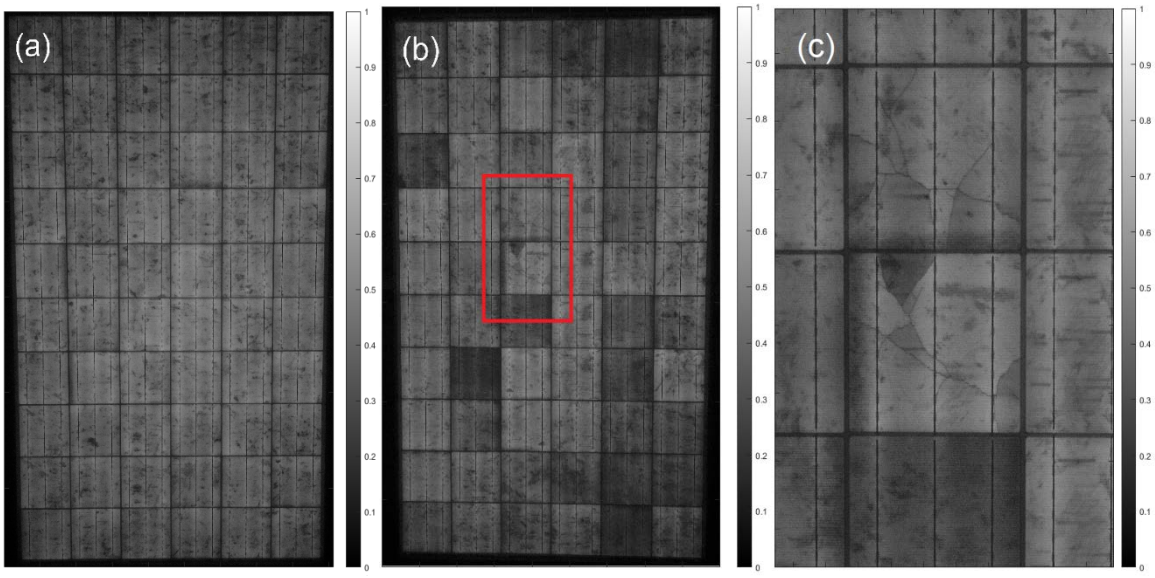

Figure 5. Electroluminescence images. (**a**) Module without defected cells, selected for the study; (**b**) non-selected module showing defects in some of its cells; (**c**) enlarged image from the red square in (**b**) to show the fractured cells of the non-select module.

A PV module consists of several layers (glass–encapsulant–cells–encapsulant–backsheet); therefore, multiple absorption losses are generated at each one [25]. These losses reduce the amount of solar irradiance reaching each PV cell. These losses are called optical losses. It is well-known that each layer is made of a material with thermal mass that causes heat to be produced in the encapsulant and to be maintained within the entire structure. This phenomenon increases the cell temperature, reduces its efficiency, and, consequently, the power of the also diminishes [26].

To determine the temperature influence on the variations of the module power and efficiency, the temperature is measured in three positions at the back of both modules (low, medium, and high). Three measurements are taken at each position and the obtained data are averaged. Comparing the records, the temperature of the lower and middle part had similar values for the clean module. When fitting the curve, they showed an intercept at (41 ± 2) °C. The high part had the lowest temperature with a value of (38 ± 2) °C. For the dirty module, the cells showed bigger differences in temperature. The cells at the low, middle, and upper positions averaged (44 ± 2) °C, (42 ± 2) °C, and (39 ± 2) °C, respectively.

In Figure 6, the measured values were compared with the calculated ones. A close relationship between the measured and expected values could actually be observed, with slopes of 0.99 ± 0.01, 0.97 ± 0.01, and 0.99 ± 0.01 for the low, middle, and upper positions in the clean module; and 1.01 ± 0.02, 0.98 ± 0.02, and 0.94 ± 0.01 for the low, middle, and upper positions in the dirty module, respectively. The slope showed values close to 1, supporting the methodology for measuring the temperature.

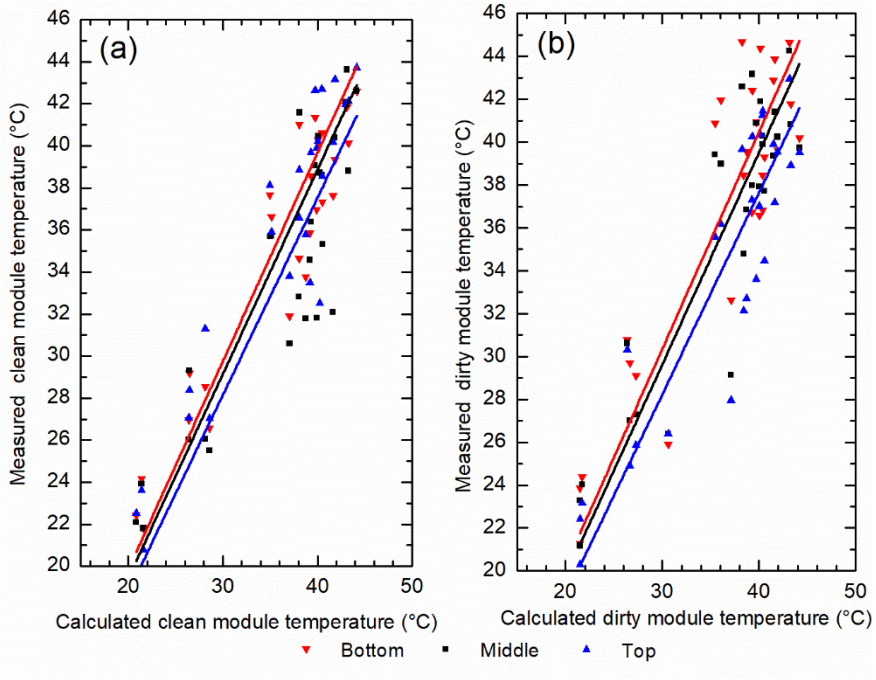

Figure 6. Plot of temperatures measured in low, middle, and upper zones, showing the calculated temperature for the same conditions in (**a**) the clean photovoltaic (PV) module and (**b**) the dirty PV module.

3.2. *Surface Dust Density*

The density of the dust deposited on the standard glass samples was measured during six months of exposure. The sampling resolution was weekly, monthly, and cumulative. This allowed the obtainment of the detailed information on the amount of dust deposited and how it was affected by the surrounding conditions. The values obtained are shown in Figure 7.

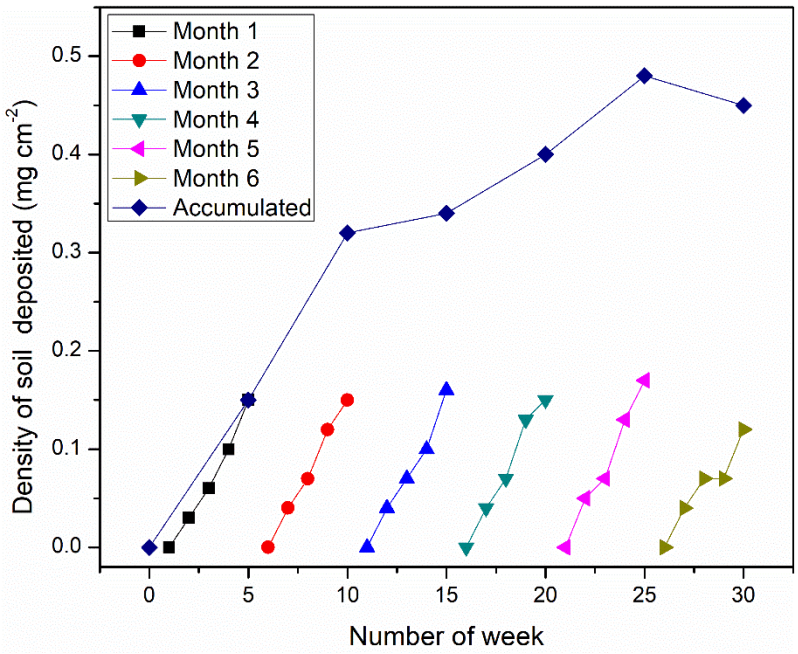

Figure 7. Density of deposited dust with weekly, monthly, and accumulated resolution for six months.

As shown in Figure 7, the monthly resolution had a maximum deposition of 0.17 mg·cm^{-2}. The deposited dust density pattern was unaltered for every month of exposure, except for the sixth one (blue), which was affected by a specific rainfall phenomenon. In this month, a maximum deposition of 0.12 mg·cm^{-2} was reached, similar to the dust density corresponding to three weeks of exposure for the previous months. Therefore, the effect of rain favored cleaning by decreasing the amount of dust corresponding to one week of exposure. For the case of accumulated dust measurements, a significant increase was observed in the first two months of exposure with values of 0.15 mg·cm^{-2} for the first month and 0.32 mg·cm^{-2} for the second one. Then, there was an increase in deposition for the remaining four months, but not as important as that compared to the first two months. This phenomenon was proposed by Akinobu Otsuka and Kotaro Iida [27], who indicated that when the dirt particles were deposited, glass–particle interaction and particle–particle interaction occurred. During the first months of exposure, the deposition was greater, due to a larger amount of available surface; where glass–particle interaction were predominant. However, as the exposure time increased, the amount of free space in which the material could be deposited decreased, causing the glass–particle interaction to be less likely to occur and the particle–particle interaction to become predominant [28–30]. Additionally, Figure 7 shows that the rain acted as a cleaning agent [9,31,32].

The values obtained for dust density were compared to the current losses generated by the soiling effects on the place. This is explained in the following section.

3.3. Electrical Performance

At the beginning of the study, both PV modules had an efficiency ~ 12.8%. On the 130th day of measurement, the efficiency of the clean module showed an increase of 5.4%$_{rel}$ (η = 13.5%), a condition that cannot be considered to be relative, since it has a daily variation of 0.0009% (R^2 = 0.99). In contrast, the dirty module reduced considerably as η = 11.5%, which was associated with a decreasing rate of 0.009% day^{-1}, as shown in Figure 8a (R^2 = 0.99).

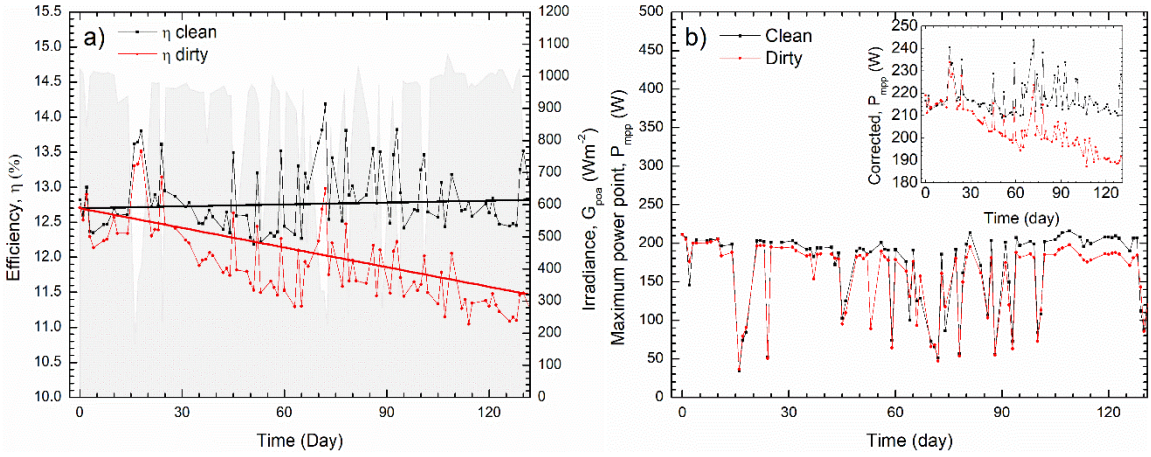

Figure 8. (**a**) Efficiency and irradiance (grey color), η ; (**b**) power at the maximum power point, P_{MPP}.

The power of both modules exhibited a behavior very similar to that of efficiency (Figure 8a,b). In both cases, the clean module followed a stationary trend, with a deviation of less than 12.5%$_{rel}$. This series was stable, with values of relative difference in power of 19.1%$_{rel}$ between the clean and the dirty modules. Complementarily, Figure 9a shows the corrected I_{sc} for the clean module to vary in 3.4%$_{rel}$. In this way, the mentioned trends allowed us to understand that there were no representative variations caused by external noise during the measurement period for the clean module. Therefore, oscillations might be produced by the climatic conditions and not by the optical agents associated with irradiance. However, the dirty module had the condition of a non-stationary series, i.e., it did not show a representative average behavior in the established period. Figure 8b shows that the corrected power of the dirty module was not stable, since its level decreased with time. The clear negative

trend could be associated with optical loss due to a decrease in the glass transmittance, driven by dust accumulation in the module, confirmed by the trend in Figure 9a [3]. Moreover, one can also observe that while the corrected power had peaks at some day, the (measured) power had valleys at the same time. This artifact was caused on low-irradiance days and it could be a consequence of the simple linear extrapolation to calculate the corrections and of the dependency of temperature coefficients to the irradiance; the larger the irradiance differed from STC, the greater the deviation in the correction [33].

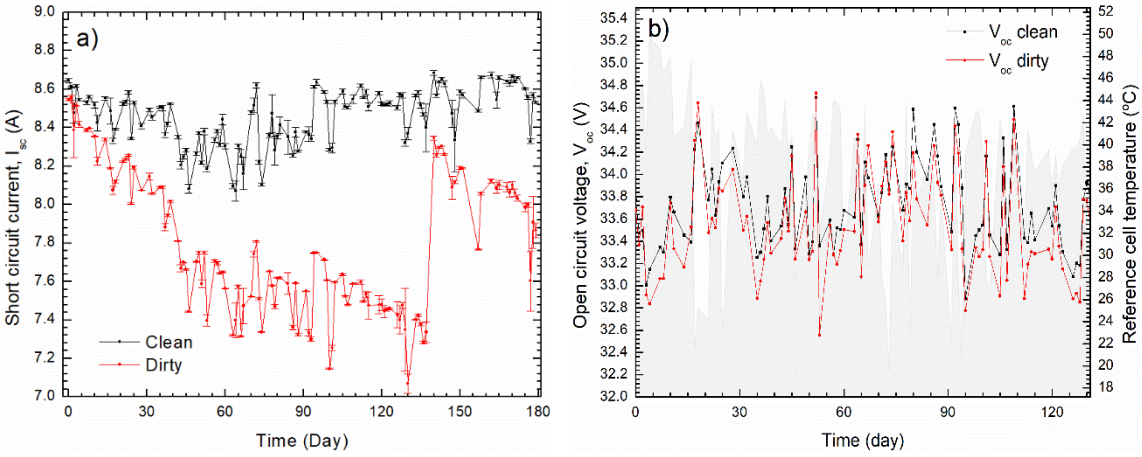

Figure 9. (**a**) Corrected values to standard testing conditions (STC) for short circuit current, I_{SC} ; (**b**) open circuit voltage, V_{OC}, and measured reference cell temperature (grey color).

Similar to the clean one, the dirty module showed oscillation in the efficiency, mainly caused by variations in the ambient conditions such as temperature. This could be confirmed by the oscillation in voltage showed in Figure 9b. Furthermore, a daily decrease in the current level by 0.01 A day^{-1} was observed for the dirty module, reaching 7.1 A at day 130.

Figure 9a shows that there was a fine relationship between optical and current losses, with a decrease rate of 0.17%/day. In contrast, the V_{OC} values indicate that the deposition did not affect the voltage. However, as shown in Figure 9b, V_{OC} shows oscillations according to temperature.

Periodical temperature changes in the module backsheet proportionately caused variations in the voltage [34].

3.3.1. Characteristic Curve

Considering the uncertainties of the characteristic IV curve, comments were independently made on efficiency (η), power (P_{mpp}), current (I_{sc}), voltage (V_{oc}), and temperature, due to weather conditions and intrinsic soiling in both studied modules. This section discusses *FF* as it allows to relate the current and voltage contributions, according to the changes shown in Figure 10, through the form of the characteristic curve.

The PV module performance parameters relate voltage V_{oc} to current I_{sc}. Thus, an IV curve was obtained, decreasing in amplitude as the dust layer density increased, which might increase or decrease *FF*, depending on how the form of the curve changed. This parameter was dependent on solar irradiance [35]. A lower *FF* resulted from the impact of the crystal soiling produced by solid microparticles deposited on the module surface. This effect decreased the shunt resistance (produced by impurities in the material) of the cells, and consequently increasing the current circulating through the material. This current was dissipated by the cell, producing heat [36]. On the other hand, the non-homogeneous shading distribution produced by soiling generated hotspots in the module, which might result in solar cell degradation [37]. In this experiment, when both modules were clean, the average *FF* was 70.8 ± 0.1%. After 130 days of measurement, the average *FF* of the module that remained clean was 70.7 ± 0.1%, while the dirty module *FF* was 72.8 ± 0.1%. The *FF* increase of the dirty module was the result of a decrease of the irradiance transmitted through the crystal. For measurement

130, there was a clear difference in the dirty module current amplitude, i.e., 12% lower than day 1. *FF* increased to 72.76%, but its efficiency decreased to 11.57%.

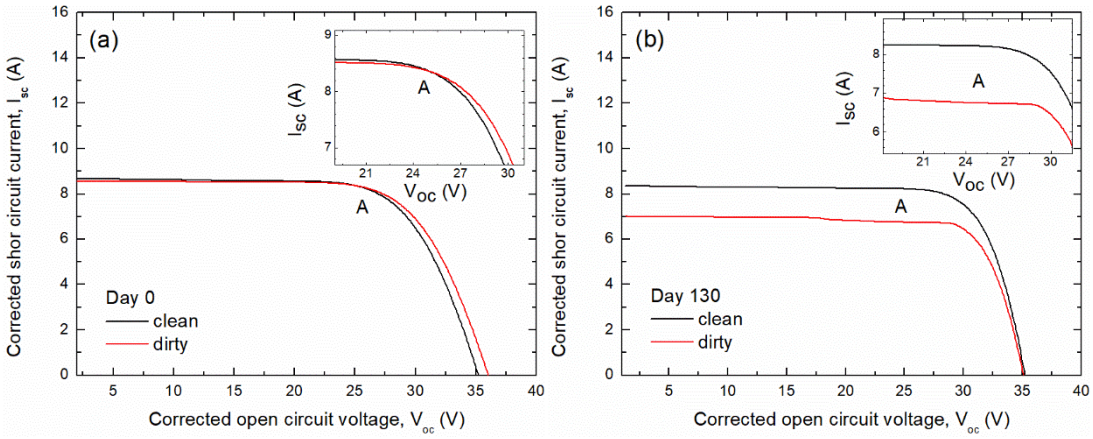

Figure 10. (**a**) Characteristic curve for the measurement of day 1. Small differences are observed. (**b**) Characteristic curve for the measurement of day 130. The distance in the curve amplitude is more highlighted.

From Figure 10b, a small jump in current for the dirty module at approximately 18 V is noticeable. After a visual inspection of the module and its IV curves, for several days, it was concluded that such an effect was caused by a bird dropping on a small portion of the glass surface of the module, causing a slight shading effect but not one significant enough to switch on the bypass diode.

3.3.2. Sky Condition Effects on Electrical Performance

Calculations of the cloudiness index in the Atacama Desert performed on the basis of more than 10 years of retrieved data [38] showed that in its vast extension, crossing the coastal mountains from west to east (see the cross-section in Figure 2a), the cloudiness index was below 3%; whereas the cloudiness index for the coastal area could rise to 45%. Together with the presence of marine aerosols, the environmental conditions in the coastal zone of Atacama Desert were more variable than, for instance, the inter depression (see Figure 2a). Consequently, there was a need to implement techniques to take cloudy and rainy days into consideration and quantify the impact on PV modules at this location.

Due to the cloudy and rainy days, the module efficiency changed, because irradiance and temperature decreased. To further describe the characteristic curve of the short circuit current during the research period, days were classified according to the atmospheric state at each moment. Therefore, considering the cloudy cover of the sky, the measurement moments corresponded to cloudless, partially cloudy, and overcast sky. To determine each moment, a sky camera was installed on the roof the Engineering Department building on the UA campus, at a short distance from the PV panels used in this study. From a total of 179 days, 53 were cloudless, 89 partially clouded, and 37 overcast. Figure 11 shows two examples for the classification of the type of sky, based on the sky camera located at UA.

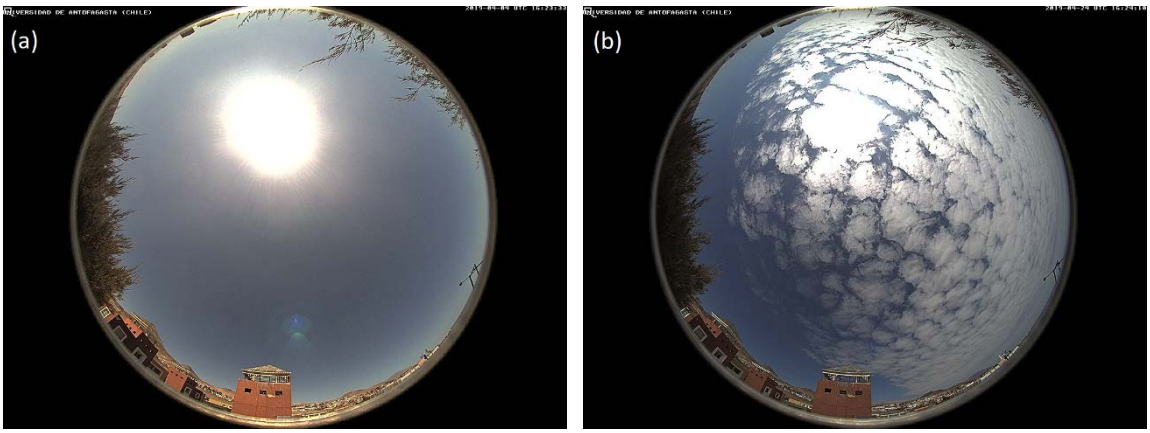

Figure 11. Images from the sky camera at Universidad de Antofagasta, showing a clear day (**a**) and an overcast day (**b**).

As the sky camera shows (Figure 11), the two moments captured were opposed in condition, since the first image illustrated a sky free of clouds, while the second one showed a thoroughly overcast sky.

Figure 12a shows the monthly efficiency variations in two PV multi crystalline modules, a clean one for each day of measurement and another one thoroughly exposed to soiling. During the first month, 47% of the days were partially clouded (May, fall); for the dirty module, the I_{sc} decreased by 6.36%$_{rel}$ and efficiency increased by 4.58%$_{rel}$ with respect to the clean module. During the next month (June, fall) there were more overcast days (42%). In this period, module efficiency already decreased by 9.37%$_{rel}$, as compared to the clean module. The current decreased by 12.63%$_{rel}$ and efficiency by 6.55%$_{rel}$. As for the previous month, current loss increased by 6.43%$_{abs}$, but efficiency differed by 1.18%$_{abs}$. Although the current was affected by optical loss, the mean temperature of the month was 20.88 °C, fluctuations were only observed at module voltage levels, which generally remained constant. In July (at the end of fall and the beginning of winter), the sky was mainly covered by clouds (55%); the current dropped by 16.37%$_{rel}$; and efficiency by 8.60%$_{rel}$. Current loss decreased by 3.74%$_{abs}$, while efficiency varied only in 2.05%$_{abs}$. After measuring 100 days, losses were only caused by soiling, while low temperatures helped to keep the voltage nearly constant (the greatest voltage levels were registered until the beginning of the next month). In August (winter), with 65% of partially clouded days, important points were observed because the current and efficiency decreased by 17.7%$_{rel}$ and 9.62%$_{rel}$, respectively. Optical losses started remaining almost constant and, as compared to the previous month, only 1.03%$_{abs}$ of the current decreased, while efficiency was even more affected, decreasing by 1.03%. The dirty module voltage decreased, showing a 1.2% negative slope, while the current remained relatively constant. This condition explained the efficiency decrease. In September (at the end of the winter and the beginning of spring), 50% of the days were mainly cloudless. Due to a rainfall, the first week of the month caused the current to be 8.22 A and efficiency to be 12.57%, as compared to the clean module. Losses decreased up to the first month of measurement, obtaining a positive current and an efficiency slope (13.8%$_{abs}$ and 8.75%$_{abs}$, respectively, above the value of the previous month). October (spring) was mainly cloudless, 61.5%. The dirty module current decreased by 4.9%$_{abs}$, as compared to the clean module and, in the same way, efficiency decreased by 1.2%$_{abs}$.

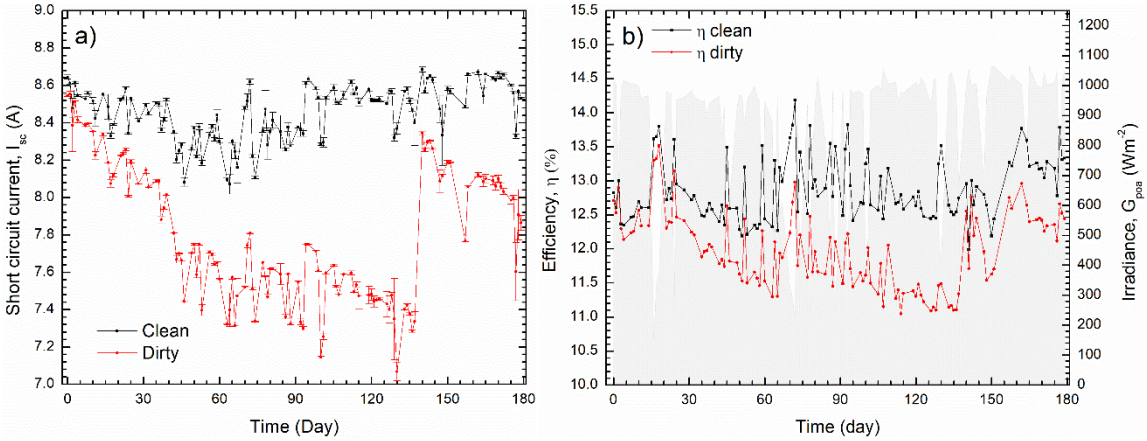

Figure 12. (**a**) Short-circuit current and (**b**) module efficiency for the measurement period, considering rainfall.

Researchers in [39] investigated the soiling in the environment of Isfahan, Iran. They studied the transmittance of glass as a function of the surface dust density in the 0.5 to 10.31 g/m^2 range. They expressed the losses in transmittance and losses in short-circuit current as a function of the amount of accumulated dust. For their first month of measurement (day 39), a difference of less than 1% was obtained between their measurements (Gholami et al. 2017) and ours, while for the days of June and August, a difference of less than 2% was obtained. July was the month that presented the greatest difference with 5%, at day 100. This simple comparison supported the statement that the measurements proposed by Gholami for the Middle East could be reproduced for other locations, as long as they were considered to be dry days, without the presence of rain. The months of September and October presented a difference of 11%, which was due to the effect of rain and its capacity to disperse dust particles to the lower edge of the module, increasing current generation and maintaining high-surface density values.

4. Conclusions

This study examined the soling impact on PV modules through means of the characteristic current–voltage (IV) curve and the density quantification of surface dust on PV glass samples. The study was conducted at the coastal zone of the Atacama Desert, where there was a direct influence of the Pacific Ocean, which was also interesting for residential applications and those on a larger scale. The procedure consisted in measuring the IV curves of a module that remained clean and another one that was not cleaned for a period of six months. PV glass samples were studied on a weekly and monthly basis, keeping track of the accumulated dust. To do this, a module selection was made by means of thermography and electroluminescence, to discard possible failure due to hotspots and broken solar cells. The conclusions for the period were as follows:

The clean module efficiency fluctuated due to irradiance and temperature variations, keeping a value of 13.01 ± 0.5%. The dirty module showed a total decrease of 9.62%$_{rel}$, dropping 0.1%$_{rel}$day^{-1}. The corrected power behaved similarly to efficiency, decreasing 0.1%$_{rel}$day^{-1} in the case of the dirty module. Current was the most affected due to soiling, with a 17.66% loss in the fourth month and a decrease of 0.14%$_{rel}$day^{-1}. After a rainfall event, loss was reduced to 3.86% as compared with day 0. The current decreased by 0.02 Aday^{-1}. The voltage between both modules did not show any significant variation.

The surface dust density increased by 0.003 mg·cm^{-2}day^{-1}. In the first five weeks, it increased more quickly (0.004 mg·cm^{-2}day^{-1}) than in later accumulation stages (0.0048 mg·cm^{-2}day^{-1} between the 6th and 10th week; 0.0034 mg·cm^{-2}day^{-1} between the 11th and 15th week; and 0.0031 mg·cm^{-2}day^{-1} between the 16th and 20th week), 0.003 mg·cm^{-2}day^{-1} between the 21st and 25th week, and 0.0025 mg·cm^{-2}day^{-1} between the 26th and 30th week of accumulation analysis.

Author Contributions: Conceptualization, P.F., A.M., J.R.-A., F.J.B., and E.F.; Data curation, D.O., J.B., M.T.-G., and J.A.-M.; Formal analysis, D.O., J.B., S.R., M.T.-G., and J.A.-M.; Funding acquisition, P.F. and A.M.; Investigation, D.O., J.B., S.R., and J.A.-M.; Methodology, D.O., P.F., S.R., A.M., J.R.-A., J.A.-M., F.J.B., and E.F.; Project administration, P.F., A.M., J.R.-A., and F.J.B.; Resources, P.F., A.M., and E.F.; Software, J.B., S.R., M.T.-G., and J.A.-M.; Supervision, D.O., P.F., S.R., A.M., J.R.-A., F.J.B., and E.F.; Validation, D.O., P.F., S.R., A.M., and F.A.-M.; Visualization, M.T.-G. and J.A.-M.; Writing—original draft, P.F. and S.R.; Writing—review & editing, P.F., A.M., and J.R.-A. All authors have read and agreed to the published version of the manuscript.

Funding: This research was funded by GORE-Antofagasta, Chile, Project FIC-R Antofagasta 2017 BIP code 30488824-0; the Chilean Economic Development Agency (CORFO) with contract No 17PTECES-75830, under the framework of the project "AtaMoS TeC"; the CONICYT/FONDECYT, grant 11190289 (Initiation in Research); CONICYT/FONDAP, grant 15110019 "Solar Energy Research Center" SERC-Chile; and the Spanish Ministry of Economy, Industry, and Competitiveness "PVcastsoil" project Nº ENE2017-83790-C3-1-2-3-R, in collaboration with the European Regional Development Fund.

Conflicts of Interest: The authors declare no conflict of interest.

References

1. Marzo, A.; Ferrada, P.; Beiza, F.; Besson, P.; Alonso-Montesinos, J.; Ballestrín, J.; Román, R.; Portillo, C.; Escobar, R.; Fuentealba, E. Standard or local solar spectrum? Implications for solar technologies studies in the atacama desert. *Renew. Energy* **2018**, *127*, 871–882. [CrossRef]
2. Ferrada, P.; Olivares, D.; Del Campo, V.; Marzo, A.; Araya, F.; Cabrera, E.; Llanos, J.; Correa-Puerta, J.; Portillo, C.; Silva, D.R.; et al. Physicochemical characterization of soiling from photovoltaic facilities in arid locations in the atacama desert. *Sol. Energy* **2019**, *187*, 47–56. [CrossRef]
3. Olivares, D.; Trigo-González, M.; Marzo, A.; Ferrada, P.; Llanos, J.; López, G.; Polo, J.; Alonso-Montesinos, J. Analysis of the Local Factors that Influence the Cementation of Soil and Effects on PV Generation at the Plataforma Solar del Desierto de Atacama, Chile. In Proceedings of the ISES Solar World Congress 2019/IEA SHC International Conference on Solar Heating and Cooling for Buildings and Industry 2019, Santiago de Chile, Chile, 4–7 November 2019. [CrossRef]
4. El-Shobokshy, M.S.; Hussein, F.M. Effect of dust with different physical properties on the performance of photovoltaic cells. *Sol. Energy* **1993**, *51*, 505–511. [CrossRef]
5. Smestad, G.P.; Germer, T.A.; AlRashidi, H.; Fernández, E.F.; Dey, S.; Brahma, H.; Sarmah, N.; Ghosh, A.; Sellami, N.; Hassan, I.A.I.; et al. Modelling photovoltaic soiling losses through optical characterization. *Sci. Rep.* **2020**, *10*, 1–13. [CrossRef]
6. Ghenai, C.; Salameh, T.; Merabet, A. Technico-economic analysis of off grid solar PV/fuel cell energy system for residential community in desert region. *Int. J. Hydrogen Energy* **2020**, *45*, 11460–11470. [CrossRef]
7. Nepal, P.; Korevaar, M.; Ziar, H.; Isabella, O.; Zeman, M. Accurate soiling ratio determination with incident angle modifier for PV modules. *IEEE J. Photovoltaics* **2018**, *9*, 295–301. [CrossRef]
8. Figgis, B.; Ennaoui, A.; Figgis, B.; Javed, W.; Chen, E. Outdoor soiling microscope for measuring particle deposition and resuspension. *Sol. Energy* **2016**, *137*, 158–164. [CrossRef]
9. Said, S.A.; Hassan, G.; Walwil, H.M.; Al-Aqeeli, N. The effect of environmental factors and dust accumulation on photovoltaic modules and dust-accumulation mitigation strategies. *Renew. Sustain. Energy Rev.* **2018**, *82*, 743–760. [CrossRef]
10. Qasem, H.; Betts, T.R.; Müllejans, H.; Albusairi, H.; Gottschalg, R. Dust-induced shading on photovoltaic modules. *Prog. Photovoltaics Res. Appl.* **2012**, *22*, 218–226. [CrossRef]
11. Maghami, M.R.; Hizam, H.; Gomes, C.; Radzi, M.M.; Rezadad, M.I.; Hajighorbani, S. Power loss due to soiling on solar panel: A review. *Renew. Sustain. Energy Rev.* **2016**, *59*, 1307–1316. [CrossRef]
12. Shaju, A.; Chacko, R. Soiling of photovoltaic modules—Review. *IOP Conf. Ser. Mater. Sci. Eng.* **2018**, *396*, 012050. [CrossRef]
13. Fuentealba, E.; Marzo, A.; Rabanal-Arabach, J.; Ferrada, P.; Araya, F. Performance analysis of photovoltaics systems installed at different sites in the atacama desert. In Proceedings of the 32nd EU PVSEC, Munich, Germany, 20–24 June 2016; pp. 1635–1640. [CrossRef]
14. Ferrada, P.; Araya, F.; Marzo, A.; Fuentealba, E. Performance analysis of photovoltaic systems of two different technologies in a coastal desert climate zone of chile. *Sol. Energy* **2015**, *114*, 356–363. [CrossRef]
15. Dupré, O.; Vaillon, R.; Green, M. Physics of the temperature coefficients of solar cells. *Sol. Energy Mater. Sol. Cells* **2015**, *140*, 92–100. [CrossRef]

16. Rabanal-Arabach, J. Development of a c-Si Photovoltaic Module for Desert Climates. Ph.D. Thesis, University of Konstanz, Konstanz, Germany, 2019.
17. Kottek, M.; Grieser, J.; Beck, C.; Rudolf, B.; Rubel, F. World map of the Köppen-Geiger climate classification updated. *Meteorol. Z.* **2006**, *15*, 259–263. [CrossRef]
18. Cruz Silva, J.C.S.C. Guía climática práctica, dirección meteorológica de Chile. In *Santiago de Chile*; DGAC Chille: Santiago, Chile, 2008.
19. Montecino, V.; Lange, C.B. The humboldt current system: Ecosystem components and processes, fisheries, and sediment studies. *Prog. Oceanogr.* **2009**, *83*, 65–79. [CrossRef]
20. McKay, C.P.; Friedmann, E.I.; Gómez-Silva, B.; Cáceres-Villanueva, L.; Andersen, D.T.; Landheim, R. Temperature and moisture conditions for life in the extreme arid region of the atacama desert: Four years of observations including the El Niño of 1997–1998. *Astrobiology* **2003**, *3*, 393–406. [CrossRef]
21. Bull, A.T.; Andrews, B.A.; Dorador, C.; Goodfellow, M. Introducing the Atacama desert. *Antonie Leeuwenhoek* **2018**, *111*, 1269–1272. [CrossRef]
22. Trigo, M.; Batlles, F.; Alonso-Montesinos, J.; Ferrada, P.; Del Sagrado, J.; Martínez-Durbán, M.; Cortes, M.; Portillo, C.; Marzo, A. Hourly PV production estimation by means of an exportable multiple linear regression model. *Renew. Energy* **2019**, *135*, 303–312. [CrossRef]
23. AERONET Aerosol Optical Depth Data Display Interface. Available online: https://aeronet.gsfc.nasa.gov/cgibin/data_display_aod_v3?site=PSDA_Chile&nachal=0&year=2019&month=4&day=30&aero_water=0&level=1&if_day=0&if_err=0&place_code=10&DATA_TYPE=0&year_or_month=3 (accessed on 22 November 2019).
24. Dierauf, T.; Growitz, A.; Kurtz, S.; Hansen, C. Weather-corrected performance ratio. *Weather Corr. Perform. Ratio* **2013**. [CrossRef]
25. Vogt, M.R.; Holst, H.; Schulte-Huxel, H.; Blankemeyer, S.; Witteck, R.; Hinken, D.; Winter, M.; Min, B.; Schinke, C.; Ahrens, I.; et al. Optical constants of UV transparent EVA and the impact on the PV module output power under realistic irradiation. *Energy Proc.* **2016**, *92*, 523–530. [CrossRef]
26. Aly, S.P.; Ahzi, S.; Barth, N. Effect of physical and environmental factors on the performance of a photovoltaic panel. *Sol. Energy Mater. Sol. Cells* **2019**, *200*, 109948. [CrossRef]
27. Otsuka, A.; Iida, K.; Danjo, K. NII-electronic library service. *Chem. Pharm. Bull.* **1988**, *36*, 741–749. [CrossRef]
28. Figgis, B.; Ennaoui, A.; Ahzi, S.; Rémond, Y. Review of PV soiling particle mechanics in desert environments. *Renew. Sustain. Energy Rev.* **2017**, *76*, 872–881. [CrossRef]
29. Ilse, K.K.; Werner, M.; Naumann, V.; Figgis, B.W.; Hagendorf, C.; Bagdahn, J.; Bagdahn, J. Microstructural analysis of the cementation process during soiling on glass surfaces in arid and semi-arid climates. *Phys. Status Solidi (RRL) Rapid Res. Lett.* **2016**, *10*, 525–529. [CrossRef]
30. Said, S.A.; Walwil, H.M. Fundamental studies on dust fouling effects on PV module performance. *Sol. Energy* **2014**, *107*, 328–337. [CrossRef]
31. Sayyah, A.; Horenstein, M.N.; Mazumder, M.K. Energy yield loss caused by dust deposition on photovoltaic Panels. *Sol. Energy* **2014**, *107*, 576–604. [CrossRef]
32. Figgis, B.; Nouviaire, A.; Wubulikasimu, Y.; Javed, W.; Figgis, B.; Ait-Mokhtar, A.; Belarbi, R.; Ahzi, S.; Remond, Y.; Ennaoui, A. Investigation of factors affecting condensation on soiled PV modules. *Sol. Energy* **2018**, *159*, 488–500. [CrossRef]
33. Dupre, O.; Vaillon, R.; Green, M.A. Experimental assessment of temperature coefficient theories for silicon solar cells. In Proceedings of the IEEE 42nd Photovoltaic Specialist Conference (PVSC), Portland, OR, USA, 14–19 June 2015; Institute of Electrical and Electronics Engineers (IEEE): Piscataway, NJ, USA, 2015; Volume 6, pp. 1–3. [CrossRef]
34. Carrero, C.; Amador, J.; Arnaltes, S. A Single procedure for helping PV designers to select silicon PV modules and evaluate the loss resistances. *Renew. Energy* **2007**, *32*, 2579–2589. [CrossRef]
35. King, D.L.; Boyson, W.E.; Kratochvill, J.A. SANDIA REPORT Photovoltaic Array Performance Model. Available online: https://prod-ng.sandia.gov/techlib-noauth/access-control.cgi/2004/043535.pdf (accessed on 23 July 2020).
36. Letin, V.A.; Nadiradze, A.B.; Novikov, L.S. Analysis of solid microparticle influence on spacecraft solar arrays. In Proceedings of the 31st Photovoltaic Specialists Conference, Lake Buena Vista, FL, USA, 3–7 January 2005; pp. 862–865. [CrossRef]

37. Kim, K.; Seo, G.-S.; Cho, B.-H.; Krein, P.T. Photovoltaic hot-spot detection for solar panel substrings using AC parameter characterization. *IEEE Trans. Power Electron.* **2016**, *31*, 1121–1130. [CrossRef]
38. Marzo, A.; Zarzalejo, L.F.; Ibarra, M.; Navarro, A.A.; Soto, G.; Ramírez, L.; Escobar, R.; Silva-Pérez, M. Towards the chilean solar thermal potential knowledge for solar power tower plants. *AIP Conf. Proc.* **2018**, *2033*, 170008. [CrossRef]
39. Gholami, A.; Saboonchi, A.; Alemrajabi, A.A. Experimental study of factors affecting dust accumulation and their effects on the transmission coefficient of glass for solar applications. *Renew. Energy* **2017**, *112*, 466–473. [CrossRef]